Kilohertz Electrical Stimulation Nerve Conduction Block: Effects of Electrode Surface Area

Yogi A. Patel, *Student Member, IEEE*, Brian S. Kim, William S. Rountree, and Robert J. Butera, *Senior Member, IEEE*

***Abstract*— Kilohertz electrical stimulation (KES) induces repeatable and reversible conduction block of nerve activity and is a potential therapeutic option for various diseases and disorders resulting from pathological or undesired neurological activity. However, successful translation of KES nerve block to clinical applications is stymied by many unknowns, such as the relevance of the onset response, acceptable levels of waveform contamination, and optimal electrode characteristics. We investigated the role of electrode geometric surface area on the KES nerve block threshold using 20- and 40-kHz current-controlled sinusoidal KES. Electrodes were electrochemically characterized and used to characterize typical KES waveforms and electrode charge characteristics. KES nerve block amplitudes, onset duration, and recovery of normal conduction after delivery of the KES were evaluated along with power requirements for effective KES nerve block. Results from this investigation demonstrate that increasing electrode geometric surface area provides for a more power-efficient KES nerve block. Reductions in block threshold by increased electrode surface area were found to be KES-frequency-dependent, with block thresholds and average power consumption reduced by greater than two times with 20-kHz KES waveforms and greater than three times for 40-kHz KES waveforms.**

***Index Terms*— Electrical stimulation, nerve block, neuromodulation, energy, power, neural interfaces, electrode, kilohertz high frequency alternating current, KHFAC, HFAC, KES.**

I. Introduction

KILOHERTZ electrical stimulation (KES) nerve block has been demonstrated in a variety of animal models and nerve diameters, including sea slugs [1], frogs [2], [3], rats [4]–[6], cats [7], [8] dogs [9], goats [10], pigs [11], and non-human primates [12]. These studies have demonstrated the ability to achieve a quick, reversible, localized block of peripheral nerve activity.

Experimental investigations using KES nerve block typically modulate two key KES parameters to achieve a complete nerve block frequency and amplitude. Previous studies have demonstrated that frequencies greater than 5 kHz are required to achieve a true conduction block [13] that is localized to the site of KES delivery, rather than neuromuscular depletion (fatigue) [2]. Frequencies as high as 70 kHz are effective experimentally [4], while frequencies up to 100 kHz have been evaluated in computational studies [14]. The KES amplitude, typically reported with units of either voltage (volts, V) or current (milliamps, mA) depending on the mode of stimulation, is determined by the target nerve's anatomy, electrical coupling between the interface and target nerve, resolution of the readout used for validation of KES nerve block, and neural interface geometry and configuration. The lowest amplitude (V or mA) at a given KES frequency that provides block of target nerve activity is referred to as the block threshold, and has been found to increase linearly with frequency for large diameter fibers and non-monotonically for small diameter fibers [1], [3], [4], [15].

Early studies report that the quality of KES nerve block is significantly impacted by the electrode configuration [16]. A few follow up investigations have been conducted recently with a focus on determining the optimal inter-pole spacing within a bipolar cuff electrode that minimizes the block threshold [17] and the onset response [18], which is a measurable burst of asynchronous nerve activation that occurs when KES delivery is initiated. Aside from the few investigations cited here, no systematic investigation has been carried out to understand the effects of electrode characteristics on KES nerve block. Furthermore, almost all published results have reported the use of different interfaces (as shown in Table I). These reports differ in electrode type, materials, and geometry, as well as animal model and target nerve, with many publications missing sufficient details to enable valuable comparison.

The focus of the present study is to systematically evaluate the effect of electrode contact geometric surface area (GSA) on KES nerve block thresholds and power consumption. The

Manuscript received November 4, 2016; revised February 10, 2017 and February 26, 2017; accepted March 6, 2017. Date of publication March 17, 2017; date of current version October 23, 2017. This work was supported in part by the Georgia Tech TI:GER Program (YAP) and in part by the NIH under Grant 2R01EB016407 (subcontract to RJB).

Y. A. Patel is with the Bioengineering Graduate Program, Georgia Institute of Technology, Atlanta, GA 30332 USA, and also with the Department of Biomedical Engineering, Georgia Institute of Technology, Atlanta, GA 30332 USA (e-mail: yapatel@gatech.edu).

B. S. Kim is with the Department of Biomedical Engineering, Georgia Institute of Technology, Atlanta, GA 30332 USA.

W. S. Rountree is with the Department of Mechanical Engineering, Georgia Institute of Technology, Atlanta, GA 30332 USA.

R. J. Butera is with the Bioengineering Graduate Program, Georgia Institute of Technology, Atlanta, GA 30332 USA, also with the Department of Biomedical Engineering, Georgia Institute of Technology, Atlanta, GA 30332 USA, and also with the School of Electrical and Computer Engineering, Georgia Institute of Technology, Atlanta, GA 30332 USA.

Digital Object Identifier 10.1109/TNSRE.2017.2684161

TABLE I
KES NERVE BLOCK INVESTIGATIONS REPORTING ELECTRODE CHARACTERISTICS (ADAPTED FROM [17] WITH PERMISSION). SINE = SEPARATED INTERFACE NERVE ELECTRODE, ND = NOT DESCRIBED

Publication	Configuration	Contacts	Conductor	Species
Cattell 1935 [19]	ND	Wires	Ag/Calomel	Frog
Rosenblut 1939 [16]	Bipolar	Wires	Ag|Ag/Cl	Cat
Reboul 1939 [20]	Bipolar	Wires	Ag|Ag/Cl	Cat
Tanner 1962 [21]	Bipolar	ND	Pt	Frog
Woo 1964 [22]	Bipolar	ND	ND	Frog/Cat
Baratta 1989 [23]	Tripolar	Wires	SS	Cat
Bowman 1986 [24]	Bipolar	Wire	Pt	Cat
Kilgore 2004 [2]	Bipolar	Wire	Pt	Frog
Tai 2004 [25]	Tripolar	Wires	SS	Cat
Bhadra 2005 [13]	Tripolar	Pads	Pt	Rat
Williamson 2005 [5]	Tripolar	Wires	SS	Rat
Bhadra 2005 [13]	Tripolar	Pads	Pt	Rat
Bhadra 2006 [7]	Tripolar	Pads	Pt	Cat
Miles 2007 [26]	Tripolar	Pads	Pt	Rat
Boger 2008 [27]	Tripolar	ND	ND	Cat
Joseph 2007 [28]	Bipolar	Wires	Ag|Ag/Cl	Sea Slug
Ackermann 2009 [17]	Bipolar	Pads	Pt	Rat
Ackermann 2010 [18]	Bipolar	Pads	Pt	Rat
Ackermann 2010 [29]	Bipolar	Pads	Pt	Rat
Gerges 2010 [30]	Bipolar	Pads	Pt	Rat
Ackermann 2010 [31]	Bipolar	Wires	W	Rat
Ackermann 2011 [32]	Monopolar	Pads	Pt+Ag|Ag/Cl	Rat
Ackermann 2011 [12]	Bipolar	Pads	Pt	Rat
Ackermann 2011 [33]	Monopolar SINE	Pads	Pt	Rat
Ackermann 2011 [34]	Bipolar	Pads	Pt	Non-Human Primate
Joseph 2009 [1]	Bipolar	Wires	Ag|Ag/Cl	Sea Slug
Joseph 2011 [3]	Bipolar	Wires	Ag|Ag/Cl	Sea Slug
Liu 2013 [35]	Bipolar	Wires	Ag|Ag/Cl	Frog
Patel 2015 [4]	Tripolar	Pads	Pt/Ir	Rat
Yang 2016 [36]	Tripolar	ND	ND	Frog
Patel 2016 [37]	Bipolar	Pads	Pt/Ir	Rat

secondary goal of this study is to evaluate the effect of contact GSA on the KES nerve block onset artifact as well as nerve conduction and recovery post-KES nerve block. We created and electrochemically characterized electrode contacts and computed the charge characteristics of KES waveforms. Experiments were then carried out to investigate the effects of contact GSA on KES block thresholds. We computed the power consumption of KES nerve block using the electrochemical characterization data and experimental KES nerve block thresholds.

II. METHODS

A. Animal Preparation

All animal research was approved by the Georgia Institute of Technology Institutional Animal Care and Use Committee. Experiments were conducted on tibial nerves from *in vivo* urethane-anesthetized rats (377.3 ± 72g, n = 6 males). Animals were briefly anesthetized using isoflurane in oxygen (5%, 1 liter/min flow rate) prior to delivery of urethane (IP, 1.2 g/kg in 0.9% saline). Anesthetic depth was evaluated 60 - 90 minutes post-injection by pinching the rear footpad and supplemental urethane (0.12 mg/ml) was delivered as necessary until the reflex withdrawal was eliminated. After reaching surgical depth, the animal's back was shaved from the lumbar section down to the distal end of the gastrocnemius muscle. The animal's foot was magnetically clamped to the surgical table to minimize motion during experimental trial. An incision approximately 1 - 1.5 cm in length was made along the length of the biceps femoris muscle and the sciatic nerve exposed via blunt dissection. The tibial branch of the sciatic nerve was identified and isolated from the sciatic notch down to the gastrocnemius muscle under a high magnification dissection scope. The common peroneal, sural, and collateral branches of the sciatic were cut to minimize off-target stimulation. Normal rat ringer's solution [38] was applied throughout the experiment to prevent muscle and nerve tissue dehydration. The animal's body temperature was monitored and maintained at 37 - 40 °C with a rectal temperature probe (Model BAT-12, Physitemp Instruments, Clifton, NJ) and warming pad (COM-11289, SparkFun Electronics, Niwot, CO). Preparations lasted 5 - 6 hours after which animals were euthanized via an IP injection of pentobarbital-based euthanasia drug (0.5 ml/kg, IP). All experiments were conducted at room temperature.

B. Electrophysiology Setup

The proximal end of the exposed sciatic nerve was stimulated using a bipolar cuff electrode made in-house. Two braided stainless steel wires (#793500, A-M Systems, Sequim, WA) separated by 1 mm were threaded through silicone tubing (#807600, A-M Systems, Sequim, WA). The wires were deinsulated inside the cuff and impedance measured at 1 kHz in 0.9% saline (Table II). A second bipolar stimulation cuff electrode was placed approximately 0.2 cm distal to the block electrode in all experiments for delivery of distal test stimuli. Distal test stimuli verified that KES nerve block was

TABLE II
IDEAL AND ACTUAL ELECTRODE CONTACT DIMENSIONS AND GEOMETRIES

Ideal Contact Dimensions (mm)	0.50 x 0.50	0.50 x 1.00	0.50 x 2.00
Actual Contact Dimensions (mm)	0.50 x 0.50 ± 0.01	0.50 x 1.00 ± 0.01	0.50 x 2.00 ± 0.03
Ideal Contact GSA (cm^2)	0.0025	0.0050	0.0100
Actual Contact GSA (cm^2)	0.0025	0.0050	0.0103
Mean Impedance at 1 kHz (kΩ)	5.54 ± 1.60	2.56 ± 0.60	1.06 ± 0.10
Number of measurements (n)	6	7	7

localized to the site of the block electrode and did not cause neuromuscular fatigue or neurotransmitter depletion.

Block of the tibial nerve was achieved using Pt/Ir (90/10, 25.4 μm thick) contact pads (ESPI Metals, Ashland, OR) spot-welded to braided stainless steel wire. Contact pads were cut and measured under a high resolution microscope with digital calipers (Table II, measurement error = 0.01), wrapped around the tibial nerve under a dissection microscope, and insulated using silicone (Kwik-Cast, WPI, Sarasota, FL). The width of all contacts was 0.5 mm. Contact lengths were chosen to provide ~90°, ~180°, and ~360° coverage (Fig. 1A) based upon a tibial nerve circumference of 2.0 - 2.1 mm [39]. Actual contact GSAs were calculated using measured mean contact dimensions. Impedance measurements were made at 1 kHz in room temperature saline stirred at a constant rate. Values shown are mean ± standard deviation. All calculations requiring contact GSA were conducted using ideal values.

Spacing between the proximal stimulation and block electrodes was approximately 1 cm in all experiments. EMG activity was differentially measured from the gastrocnemius muscles using bipolar fine wire electrodes (Cooner Wire No. AS631, Chatsworth, CA). EMG measurements were filtered (100 - 300 Hz) and gained (1000x, Brownlee Precision Model 440, San Jose, CA) before being digitized at a rate of 20 kHz using The Real-Time eXperiment Interface (RTXI [56], http://www.rtxi.org) with a PCI-6036E data acquisition card (National Instruments, Austin, TX). A stainless steel wire was inserted into the contralateral gastrocnemius muscle and connected to the surgical air table to electrically ground the animal, with the surgical table grounded to the amplifier (building supply ground). Figure 1B shows the complete experiment setup.

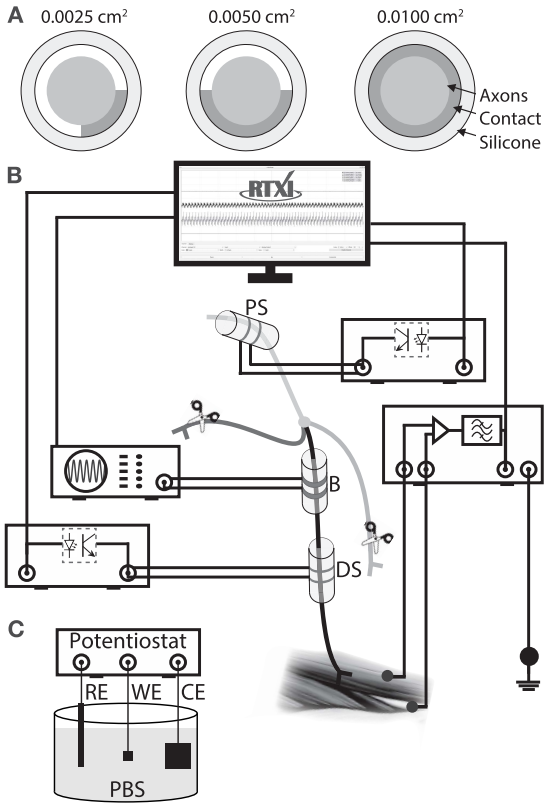

Fig. 1. Electrophysiology setup and electrode configurations. (A) Illustration of increasing nerve coverage with increasing contact GSA. (B) The nerve was electrically stimulated at the proximal and distal ends using bipolar cuff electrodes. EMG activity was measured from the gastrocnemius muscle using intramuscular fine wire electrodes. KES nerve block was delivered proximal to the distal stimulation electrode using a bipolar cuff electrode. Timing and duration of stimulation events, along with measurement of activity was achieved with RTXI. PS = proximal stimulation electrode, B = Block electrode, DS = distal stimulation electrode. (C) Three electrode setup used for electrochemical characterization, RE = reference electrode,WE = working electrode, CE = counter electrode.

C. Nerve Activation and KES Block

Constant current pulses (0.3-0.5 mA_{peak}, 0.2 ms, 1 Hz) were generated using the RTXI signal generator module for proximal stimulation and an optically isolated constant current stimulator (DS3, Digitimer, Ft. Lauderdale, FL) for distal stimulation. Proximal stimulation pulses were optically-isolated using linear stimulus isolators (A395, WPI, Sarasota, FL). The KES waveform (current-controlled, continuous sinusoid) was generated using a floating current source function generator (Model 6221, Keithley Instruments, Inc, Clevelend, OH). The 2.1 mA_{peak} and 21.0 mA_{peak} ranges were used for the 20 kHz and 40 kHz KES trials, respectively. Direct current contamination of the KES waveform was randomly measured with a 10 Ω sense resistor in series with the return electrode and found to be 150 - 500 nA. All stimulus isolation units used were calibrated prior to each experiment and output offsets zeroed by visualization on an oscilloscope. Timing control of stimulation equipment was achieved by using digital I/O triggers generated from RTXI.

D. Experimental Protocols

The first trial was conducted to determine the block threshold with a given electrode and KES frequency (as previously described in [4]). The sciatic nerve was stimulated at 1 Hz using the proximal stimulation electrode to elicit supra-maximal EMG activity in the gastrocne-

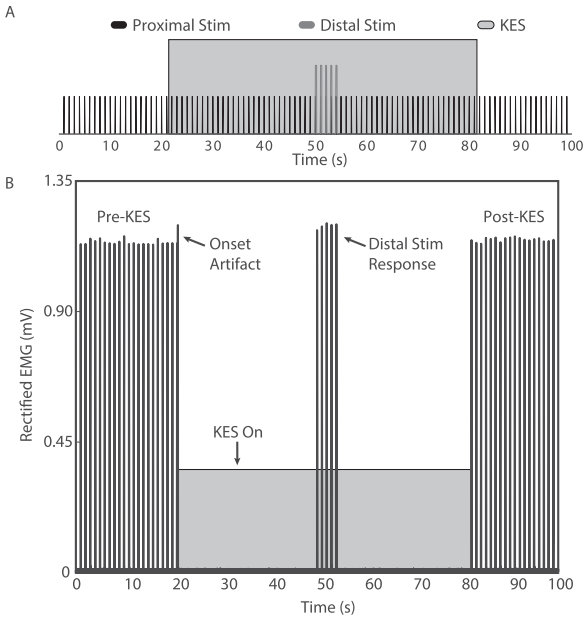

Fig. 2. Experiment trial protocol and representative data. (A) Each trial lasted a total of 100 seconds, with KES on for 60 seconds. Stimulation pulses were delivered via the proximal stimulation cuff electrode throughout the entire trial. Five stimulation pulses were delivered to the nerve via the distal stimulation electrode to assess the locality of KES nerve block. (B) Representative rectified evoked EMG data.

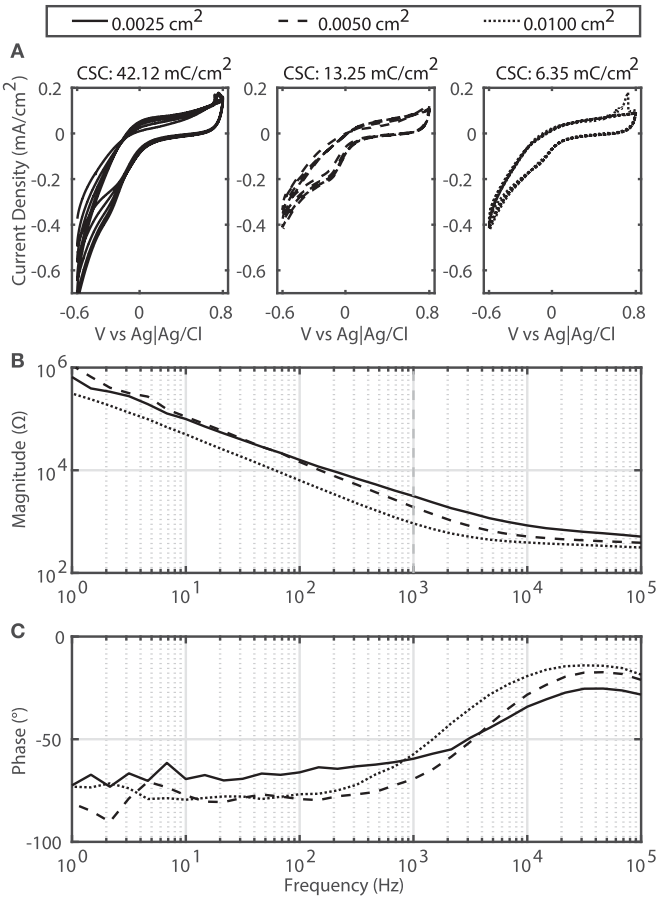

Fig. 3. Electrochemical characterization of electrodes. (A) Five voltammograms are shown for each contact GSA evaluated (increasing contact GSA from left to right). The cathodic time integral was taken for each voltammogram and averages to calculate the cathodic CSC per contact GSA. Representative electrical impedance magnitude (B) and phase angle (C) are shown for each contact GSA. Impedance magnitudes are reduced with increasing contact GSA, with a linear response at typical KES frequencies.

mius muscle. The threshold was found by increasing the amplitude of the KES waveform in 0.1 mA_{peak} increments until complete block was achieved. Complete block was achieved only when the root mean square (RMS) voltage of the EMG measurement was equivalent to that of the measurement noise. The second trial was conducted at the empirically determined block threshold, with approximately 3 - 5 minutes between each trial. In each trial, a total of 100 stimulation pulses were delivered to the nerve (Figure 2A). The initial 21 stimulation pulses were delivered to the nerve to capture pre-KES EMG activity. KES was delivered to the nerve 900 ms after the 21st stimulation pulse at either 20 or 40 kHz with the predetermined block threshold. Test pulses were delivered to the nerve while delivery of KES nerve block for continuous assessment of KES nerve block efficacy. The KES waveform was automatically turned off after 60 seconds (60 stimulation pulses) with continued nerve stimulation to measure post-KES EMG activity (18 stimulation pulses). Figure 2 provides a pictorial description of the experimental protocol for a single trial and representative data.

E. Electrochemical Measurements

Monopolar cyclic voltammetry (CV) measurements were made for electrode contacts of different GSAs to compute the cathodic charge storage capacity (CSC) (Fig. 3A). Measurements were made using a three electrode setup (Fig. 1C) with a Ag|Ag/Cl reference electrode and a Pt counter electrode (surface area: 0.02 cm^2). A potentiostat (VMP3, Bio-Logic) was used to sweep the potential between -0.6 V and 0.8 V with a scan rate of 50 mV/sec while simultaneously measuring the current flow between the working (monopolar test electrode) and counter electrodes. The negative current time integrals were computed for each voltammogram and averaged to obtain the mean cathodic CSC for each contact GSA [40].

Monopolar electrical impedance spectroscopy (EIS) measurements were made using the same three electrode setup to quantify changes at the electrode-tissue-interface as a function of contact GSA (Fig. 3B-C). Measurements were made by sweeping a 10 mV excitation waveform over a frequency range of 1 - 10^5 kHz. All electrochemical measurements were made in room temperature (25 °C) phosphate buffered saline (PBS, pH = 7.4, Sigma Aldrich, St. Louis, MO) stirred at a constant rate. The measured impedance magnitude and phase at experimentally tested KES frequencies were used for waveform and power computations.

F. Waveform Characterization

Nearly all investigations to date have presented KES nerve block data in terms of block thresholds only. We analyzed typical KES waveforms for common characteristics including charge density, current density, and charge per phase as a

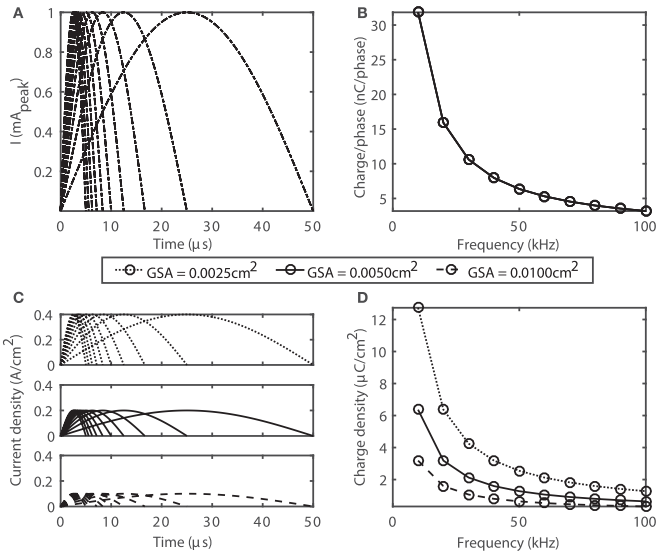

Fig. 4. Waveform characteristics for a range of KES waveform frequencies (10-100 kHz, 10 kHz steps) with an amplitude of 1mA$_{peak}$ as a function of contact GSAs. (A) Cathodic phase of each waveform was used in computations. The x-axis is the period of a single cathodic cycle at a given KES frequency. (B) Charge per phase decreases exponentially as a function of KES frequency. (C) Current densities decrease as the contact GSA increases. (D) Charge densities decrease exponentially as a function of KES frequency and and linearly decrease with increasing contact GSA.

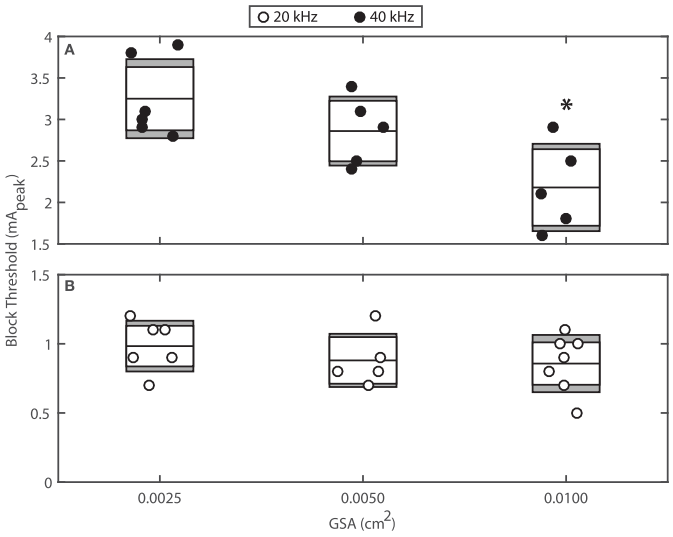

Fig. 5. KES block thresholds as a function of contact GSA for 20 and 40 kHz KES nerve block. Each circle represents an individual trial at one KES frequency. Each contact GSA group was found to be normally distributed with the equal variances (Bartlett's statistic, $p_{20kHz} = 0.96$, $p_{40kHz} = 0.91$). A one-way analysis of variance did not detect any significance between the mean =20 kHz block thresholds at all contact GSAs ($p < 0.05$), however did reveal a significant difference between the mean 40 kHz block thresholds for 0.0025 cm^2 and 0.0100 cm^2 contact GSAs ($p^* < 0.05$).

function of KES frequency and contact GSA (Fig. 4). One full period of each KES (sinusoidal) current waveform was generated in MATLAB 2016 (MathWorks Inc., Natick, MA) with a sampling rate of 20 MHz (Appendix V, Eqn. 3). The cathodic phase (Figure 4A) was used for computing waveform characteristics. Charge per phase (Fig. 4B), current density (Fig. 4C), and charge density (Fig. 4D) were calculated using equations 4, 5, and 6 (Appendix), respectively.

G. Power Calculations

We used EIS magnitude, phase, and mean KES block thresholds (Fig. 5) to approximate the energy required to achieve effective KES nerve conduction block with each contact GSA (Fig. 6). The mean RMS (mA$_{peak}$) KES block threshold for each contact GSA was used to generate a single cycle of a 20 and 40 kHz KES current waveform (Appendix V, Eqn. 3). The EIS magnitude and phase for 20 and 40 kHz were obtained by interpolating between the EIS measurements for each contact GSA. The magnitude was used to generate an equivalent voltage waveform (Eqn. 1). The phase and generated voltage and current waveforms were then used to calculate the power (Eqn. 2).

$$V_{RMS} = I_{RMS} * |Z(GSA, KES)| \quad (1)$$

$$Power = V_{RMS} * I_{RMS} * cos(\phi) \quad (2)$$

H. Data Analysis

All data were analyzed with MATLAB. EMG recordings were detrended and windowed (10 ms bins) to capture evoked EMG activity. The stimulus trigger was used to define the EMG window's left edge. An additional 10 ms window was used to capture baseline noise prior to stimulus delivery. The windowed data was full-wave rectified and the RMS voltage used as a metric for evaluating nerve and muscle activation as well as KES nerve block. The noise RMS voltage was subtracted from the EMG RMS voltage to reduce variance introduced by noise and differences in electrical coupling between experimental setups. Onset artifacts were identified by comparing the RMS voltage of a moving 10 ms window to pre-KES RMS noise values. Evoked EMG latencies were calculated by subtracting the time of the stimulation trigger from the time of the evoked EMG response. Recovery times were measured as the time between turning off KES and recovery of evoked EMG magnitudes to 90% of pre-KES values. All box plots show the population mean (center black bar), 95% confidence interval (white region), and one standard deviation (gray region).

III. Results

A. Electrochemical Characterization of Electrodes

Electrochemical characterization of electrodes provides valuable information about the safety of stimulation waveforms with respect to tissue damage, electrode stability, and the response of electrodes to different stimulation waveforms. We performed CV measurements (Fig. 3A) to quantify the cathodic CSC of each GSA with previously published potential limits [40]. Cathodic CSC values were 42.12 ± 0.51 mC/cm^2, 13.25 ± 0.15 mC/cm^2, and 6.35 ± 0.09 mC/cm^2 for increasing GSA, respectively. Cyclic voltammograms for the 0.0025 cm^2 electrode demonstrated greater cycle-to-cycle variability. The cathodic CSCs decreased with increasing

contact GSAs (Fig. 3A). EIS measurements (Fig. 3B-C) provide the frequency response of each electrode across a wide range of frequencies. Increasing the contact GSA decreases the electrical impedance magnitude at all frequencies greater than 100 Hz. At KES frequencies evaluated experimentally, the impedance was 505 ± 153 Ω for 20 kHz and 457 ± 122 Ω for 40 kHz.

B. Charge Characteristics of KES Waveforms

In addition to contact GSA, minimization of power consumption requires understanding the charge characteristics of typical KES waveforms. Cogan [40] proposed charge per phase, charge density, and current density as informative metrics for characterizing neural stimulation electrodes and waveforms. We computationally characterized these metrics for a range of KES frequencies at a single amplitude (Fig. 4). As the KES frequency increases, the duration of the cathodic phase decreases (Fig. 4A), resulting in a decreased charge per phase (Fig. 4B). If the peak KES amplitude is increased, the absolute value of the charge per phase curve increases, however the exponential decrease as a function of KES frequency will remain. As the contact GSA increases, the magnitude of the current density decreases (Fig. 4C). Charge densities (Fig. 4D) exponentially decrease as a function of KES frequency, and decrease linearly as a function of contact GSA.

C. Increased GSA Reduces KES Block Thresholds and Power Consumption

Block thresholds are the primary metric reported by most KES nerve block studies. KES nerve block thresholds reported in this report (Fig. 5) demonstrate an inverse relationship with contact GSA; block thresholds decrease as contact GSA increases. Decreases in mean block threshold were not significant with 20 kHz KES waveforms, in contrast to the significant decreases seen with 40 kHz KES waveforms (Fig. 5). Average power consumption also decreased linearly as a function of contact GSA for both 20 kHz ($R^2 = 0.81$) and 40 kHz ($R^2 = 0.98$) KES waveforms.

D. Increased GSA Does Not Alter Post-KES Nerve Block Characteristics

In addition to power consumption, the clinical utility of KES nerve block may be affected by the onset response, changes in normal nerve conduction, as well as recovery of normal conduction after KES is turned off. The onset response durations (Fig. 7) were quantified as a function of KES frequency and contact GSA. No consistent difference was observed in onset duration as a function of contact GSA. Changes in EMG activation (Fig. 8) were used as a proxy to assess nerve conduction latencies pre- and post-KES nerve block. Although mean post-KES nerve block EMGs are reduced for all groups, significant variability exists, leading to no consistently identifiable change in EMG activation as a function of KES frequency or contact GSA. Nerve conduction latencies increased after delivery of KES nerve block but no consistent and reproducible change was observed. Mean post-KES latencies increase and demonstrate a wider distribution post-KES. There is no dependence upon contact GSA or KES frequency, however. Normalized EMG pre- and post-KES nerve block were used to quantify changes in the quality of recovered nerve activity after 60 seconds of complete and effective block (Fig. 9). Finally, increasing contact GSAs decreased recovery times for 20 kHz KES trials. This effect. however, is not observed for 40 kHz KES trials.

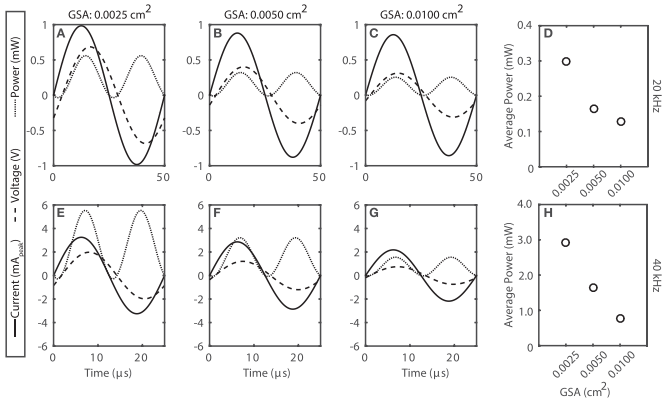

Fig. 6. Increasing contact GSA reduces the power required for effective KES nerve block. The current (mA_{peak}, solid), voltage (V, dashed), and power (mW, dotted) are shown for each GSA. Voltage and power values are derived using the mean block thresholds and EIS measurements. The power is computed for each GSA at 20 kHz (D) and 40 kHz (H) for an application duration of 60 seconds. In both 20 and 40 kHz cases, the power required to achieve an effective KES nerve block decreases with increasing contact GSA.

IV. Discussion

Interest and clinical availability of bioelectronic medicines have significantly grown in the past decade mostly due to the initiatives started by for-profit and non-profit entities. At the root of many of these initiatives is the ability to interface with the nervous system - in particular with the peripheral nervous system with the goal of monitoring and treating a variety of clinical conditions. KES nerve block offers a promising new approach for bioelectronic medicines - providing both temporal and spatial control of peripheral nerve activity. A significant number of questions remain to be answered to ensure safe and effective implementation of KES nerve block in clinical therapies - including but not limited to the optimal electrode specifications and power requirements which are the focus of the present study.

In the present study, preparations of the anesthetized rat tibial nerve were used to evaluate the effects of increasing GSA on KES nerve block thresholds. Increasing GSA was achieved by increasing the length of the electrode contacts while the width was fixed. The effect of three different contact lengths (Table II) on KES nerve block thresholds were evaluated with KES frequencies of 20 and 40 kHz. Electrode charge characteristics were computationally characterized as a function of increasing GSA and KES frequency (Fig. 4). Finally, electrodes of different GSAs were electrochemically characterized (Fig. 3) and paired with experimentally-derived

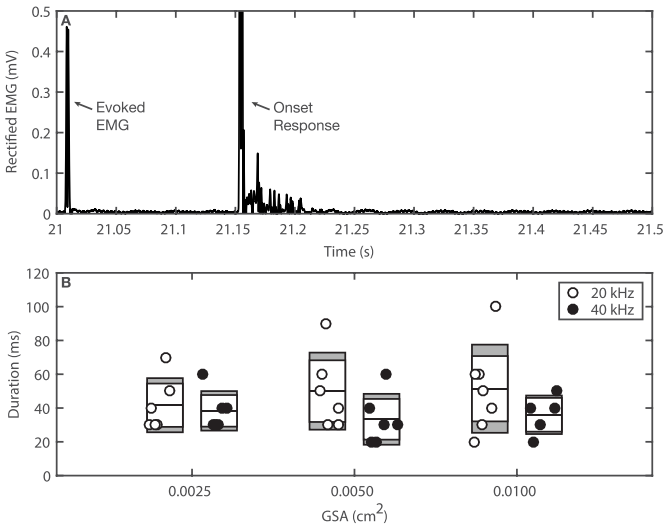

Fig. 7. Rectified EMG onset artifact durations. (A) Rectified EMG onset artifacts always followed the 21st evoked-EMG response. The onset artifact consists of a large, high-frequency transient spike in measured EMG activity followed by a brief period of spontaneous activation, followed by complete KES nerve block. (B) The width of the rectified EMG onset artifact window is used to represent the duration of the onset artifact as a function of contact GSA and KES frequency.

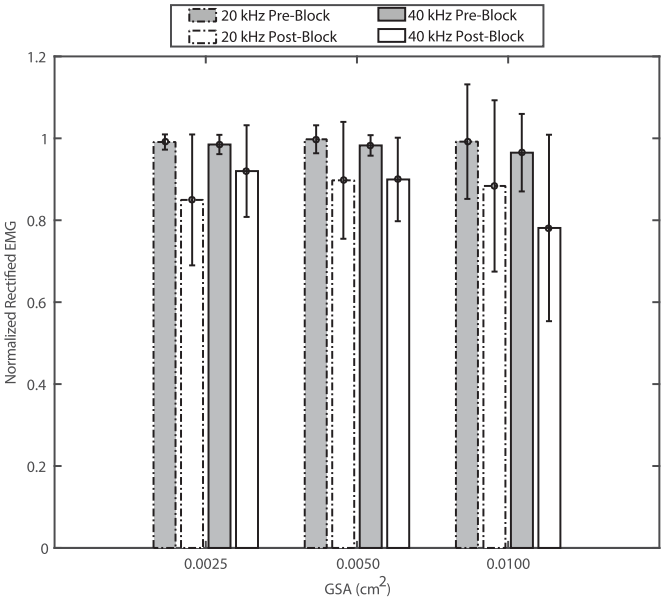

Fig. 8. Normalized rectified EMG before and after delivery of KES nerve block. Gray and white bars represent pre- and post-KES nerve block EMG values. Dashed and solid line boxes represent trials using 20 kHz and 40 kHz, respectively. One-way analysis of variance demonstrated no significant difference in pre- and post-block EMG as a function of contact GSAs.

KES nerve block thresholds to estimate the power consumption of effective KES nerve block (Fig. 6). Our results demonstrate that KES nerve block thresholds are inversely related to the electrode contact GSA (Fig. 5), and that the magnitude of this inverse relationship increases at higher KES frequencies. As the KES nerve block threshold decreases, the estimated power for effective KES nerve block also decreases (Fig. 6D and H). The inverse relationship between contact GSA and block thresholds is likely due to multiple factors - such as lower impedance magnitudes and increased electric field uniformity. Increasing GSA provides for a more power efficient KES nerve block but has no statistically significant and observable effect on the onset artifact duration, recovery, or the nerve conductivity (Figs. 7, 8).

One observation of the experimental data presented here (Figs. 5, 7, 8) is the wide range of variability in computed metrics. These experiments were performed with acute preparations which typically demonstrate a wide range of variability. This variability is inherently tied to acute experiments due to differences in the electrode-tissue interface resulting in different input-output relationships [41]. It is speculated that this variability will decrease significantly in chronic experimental evaluation. For example, the KES block thresholds (Fig. 5), although well within the published range of block thresholds at each KES frequency, might present a significantly tighter variance on a per-nerve basis once the electrode is encapsulated by fibrous tissue. It is also possible that the low levels of direct current contamination measured in our experiments contributed to the observed variability. For example, the reduction in post-KES EMG activity may be due to localized damage to axonal structures and requires histological examination. Previous investigations have been reported on the use of blocking capacitors and/or inductors to minimize direct current contamination of KES waveforms [42]. We did not employ these methods but did characterize the contamination. Our experience with blocking capacitors suggests that direct current contamination is reduced during delivery of KES. However, the capacitors discharge through the neural tissue when KES delivery is turned off, significantly damaging the underlying neural tissues. Large inductors (>5 H) provide one solution to the discharging of blocking capacitors and direct current contamination [42], but are clinically impractical.

Although not assessing contact GSA, other investigations have characterized the effects of electrode geometry, specifically spacing between electrode contacts on the KES nerve block threshold as well as the onset artifact. Ackermann *et al.* [17] investigated the effect of inter-pole distance on both KES nerve block thresholds and the onset response with results suggesting that 1 mm between poles is optimal. A number of follow-up investigations by the same group were carried out to reduce the onset response which can last up to 10 s after initiation of KES nerve block [18], [32]. However this onset artifact duration is in contrast to our findings which demonstrate (Fig. 7) that the onset response never exceeded 120 ms [4]. The longer duration onset artifacts published by others using the sciatic-gastrocnemius muscle complex preparation are likely a combination of both the neural onset (milliseconds) and physiological onset (seconds). In this case, the physiological onset is the passive relaxation properties of muscle fibers. The concept of neural vs physiological onset artifacts is an important factor that should be considered when evaluating the onset response in different neural circuits.

In addition to the short duration onset response, our experimental results demonstrate that recovery after 60 seconds

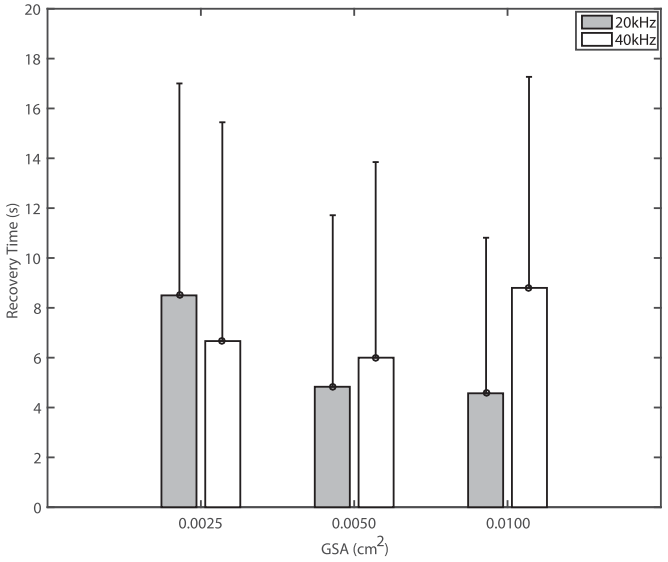

Fig. 9. Post-KES recovery time of EMG activity. Gray and white boxes represent the duration between the end of KES block delivery and recovery of EMG activity to 90% of pre-KES block values. Mean recovery times decrease as a function of contact GSA for 20 kHz KES, however the standard deviation is large and the same behavior is not observed with 40 kHz trials. One-way analysis of variance demonstrated no significant difference in recovery times as a function of contact GSAs.

of KES nerve block is nearly instantaneous with significant variability in terms of the magnitude of the recovered EMG response (Fig. 8). The variability could be due to the extremely low levels of direct current measured in our experiments, however we stimulated the nerve distal to the KES nerve block cuff electrode to validate that KES block was local to the site of the block cuff electrode and not neuromuscular fatigue or depletion block [43]. In all our trials, recovery of EMG activity was instantaneous with proximal stimulation evoked EMG measured within less than one second of turning off KES nerve block. Analysis of post-KES block EMG activity suggests that evoked EMG (resulting from nerve conduction recovery) returns to 90% of pre-KES EMG magnitude within an average of 10 seconds (Fig. 9). These post-KES recovery characteristics are similar to previous reports [35], but in conflict with others [36]. In the latter investigation, complete KES nerve block was observed up to 10 seconds after turning off KES. Although the study states the use of an electrode to stimulate the nerve distal to the block site, complete trials are not shown and twitches in response to distal stimulation are absent from force transducer measurements ([36, Figs. 2–4]), suggesting that the results maybe an artifact of neuromuscular depletion or fatigue block, rather than a true conduction block localized to the KES electrode.

The results presented here demonstrate the ability of optimized electrode GSA to minimize the power consumption of KES nerve block. This data is based upon the tibial nerve, which is a mixed nerve containing both motor (4358 $\pm$ 513 axons, 2.0 - 12.0 μm diameter) and sensory (9077 $\pm$ 1600 axons, 0.5 - 1.0 μm diameter) [39]. Efficacy of KES nerve block was assessed through measurements of supramaximal evoked EMG activity from the gastrocnemius muscle.

EMG activity can contain two identifiable waves - the M-wave and H-wave, which represent motor and sensor activity, respectively. Initial experiments attempted to measure both M- and H-wave activity to allow for assessment of both large (motor) and small (sensory) diameter axons. Unfortunately, a trade-off exists between using supramaximal stimulation to evoke maximal EMG and activation of a measurable H-reflex. With increasing stimulation intensities the M-wave increases, but the H-reflex amplitude decreases due to increased antidromic collisions [44].

For the purposes of this study, we opted for supramaximal activation of EMG activity (M-wave) to enable a thorough characterization of true, effective KES nerve block thresholds as a function of contact GSA and the corresponding power consumption. However, it is important to note that KES nerve block of small diameter fibers has been shown with high amplitudes (at KES frequencies < 30 kHz) and with lower KES amplitudes (at KES frequencies >30 kHz) [3], [4]. In cases where KES nerve block of small diameter axons is desired, such as the cervical vagus [37], optimization of contact GSA may provide significant reductions in power consumption.

Reduced power consumption of KES nerve block can significantly impact the design of clinical devices focused on effective KES nerve block. The data presented here demonstrate >2x reduction in power consumption when contact GSA is optimized and used with 20 kHz KES nerve block. Similarly, when contact GSAs are optimized for the nerve of interest, the power reductions are >3x for 40 kHz KES. In both cases the lifetime of an implanted device can be extended.

The mechanism of action of KES nerve block is unknown, with only computationally-derived hypotheses in the published literature. One computationally-derived hypothesis is that KES nerve block is achieved via inactivation of sodium channels by membrane depolarization [2], [5], [45]. In contrast, another computationally-derived hypothesis is that KES leads to elevated levels of potassium channel activation [46]–[48]. Neither of the hypothesized mechanisms have been experimentally investigated, primarily due to the difficulty associated with measurement of membrane characteristics under KES stimuli. The results from this investigation do not speak directly to the existing hypothesized mechanisms of KES nerve block, but do shed new light on appropriate computational approaches. For example, nearly all computational studies into the mechanism of KES nerve block have utilized single axon models with monopolar point sources for delivery of KES. This geometric configuration ignores the interactions between axonal elements, the electrode-tissue interface, and KES waveforms. The results from the present study suggest that geometry of the electrode plays a critical role in effective KES nerve block, and warrant the need for computational studies that include the appropriate scales, elements, and physics involved in achieving effective KES nerve block, as exemplified by recent investigations [49]–[51].

While the effects of electrode geometry have received some attention, other topics related to electrodes used for KES nerve block have not. The contacts used in this investigation were made of Pt/Ir, which has received significant attention by the neural stimulation community [52], [53]. Pt/Ir uti-

lizes both faradaic (oxidation-reduction reactions) and capacitive (electrode-electrolyte double layer charging) mechanisms to inject charge into the target neural tissues, the contribution of each mechanism depending upon the current density and the pulse width. One question of significant interest is whether or not the use of materials with different charge injection mechanisms has an effect on KES nerve block thresholds and power consumption. For example, materials such as Titanium Nitride (TiN), which delivers charge through capacitive mechanisms [54], has a high charge injection capacity, and reduced electrode polarization, may further reduce the power requirements of KES nerve block.

V. Conclusion

KES nerve conduction block is a powerful technique capable of providing fast, effective, and robust block of nerve activity. The results presented in this manuscript demonstrates one approach for reducing the power consumption of KES nerve conduction block. A small but growing number of clinical products which utilize KES exist, such as Enteromedics VBLOC [11], Neuros Altius (Neuros Medical, Inc., Cleveland, OH, USA), and Nevro HF10 [55]. It is unclear if any of these clinical products produce a true nerve conduction block via KES or if conduction block is the intended physiological response. These existing devices may be able to extend device battery life, however, and reduce or simplify recharging strategies by ensuring optimal contact GSAs and choice of KES frequency for the targets of interest.

Acknowledgment

This work was funded by the Georgia Tech TI:GER program (YAP) and NIH Grant 2R01EB016407 (subcontract to RJB). The authors thank Dr. Omer Inan for providing feedback on the power analysis. The authors also thank Dr. Laura O'Farrell for her feedback on the manuscript text and thank Dr. Manfred Franke for providing feedback and stimulating conversation on the topic of KES nerve block. Finally, this manuscript is dedicated to William S Rountree - an extremely smart, charismatic, and kind man who left the world too soon. He fabricated electrodes, supported with experiments, analyzed data, provided feedback on the manuscript, and great company - which is and will continue to be missed.

Author Contributions

YAP, BSK, and WSR designed and conceived the study. BSK and YAP performed experiments. WSR, BSK, YAP, and RJB analyzed data. BSK and WSR fabricated electrodes. WSR and YAP conducted electrochemical characterization experiments. YAP, BSK, WSR, and RJB wrote the manuscript.

Appendix
Charge Calculations

$$I(t) = I * sin(2 * \pi * f * t + \phi), \quad 0 \leq t \leq \frac{1}{T_{KES}} \tag{3}$$

$$Q_{phase} = \int_0^{\frac{1}{2}T_{KES}} I(t) \tag{4}$$

$$I_\rho(t) = \frac{I(t)}{GSA}, \quad 0 \leq t \leq \frac{1}{2}T_{KES} \tag{5}$$

$$Q_\rho = \frac{\int_0^{\frac{1}{2}T_{KES}} I(t)}{GSA} \tag{6}$$

References

[1] L. Joseph and R. J. Butera, "Unmyelinated Aplysia nerves exhibit a nonmonotonic blocking response to high-frequency stimulation," *IEEE Trans. Neural Syst. Rehabil. Eng.*, vol. 17, no. 6, pp. 537–544, Dec. 2009.

[2] K. L. Kilgore and N. Bhadra, "Nerve conduction block utilising high-frequency alternating current," *Med. Biol. Eng. Comput.*, vol. 42, no. 3, pp. 394–406, May 2004.

[3] L. Joseph and R. J. Butera, "High-frequency stimulation selectively blocks different types of fibers in frog sciatic nerve," *IEEE Trans. Neural Syst. Rehabil. Eng.*, vol. 19, no. 5, pp. 550–557, Oct. 2011.

[4] Y. A. Patel and R. J. Butera, "Differential fiber-specific block of nerve conduction in mammalian peripheral nerves using kilohertz electrical stimulation," *J. Neurophysiol.*, vol. 113, no. 10, pp. 3923–3929, 2015.

[5] R. P. Williamson and B. J. Andrews, "Localized electrical nerve blocking," *IEEE Trans. Biomed. Eng.*, vol. 52, no. 3, pp. 362–370, Mar. 2005.

[6] N. Bhadra and K. L. Kilgore, "Block of mammalian motor nerve conduction using high frequency alternating current," in *Proc. 2nd Int. IEEE EMBS Conf. Neural Eng.*, vol. 10. Mar. 2005, pp. 1–3.

[7] N. Bhadra, N. Bhadra, K. Kilgore, and K. J. Gustafson, "High frequency electrical conduction block of the pudendal nerve," *J. Neural Eng.*, vol. 3, no. 2, pp. 180–187, 2006.

[8] A. Boger, N. Bhadra, and K. J. Gustafson, "Different clinical electrodes achieve similar electrical nerve conduction block," *J. Neural Eng.*, vol. 10, no. 5, p. 056016, 2013.

[9] E. Lin, K. L. Kilgore, N. Bhadra, and E. A. Lahowetz, "Chronic high-frequency nerve block with an implanted waveform generator," in *Proc. Int. Funct. Elect. Stimulation Soc. Conf.*, 2007, p. 1.

[10] J. M. Cuellar, K. Alataris, A. Walker, D. C. Yeomans, and J. F. Antognini, "Effect of high-frequency alternating current on spinal afferent nociceptive transmission," *Neuromodulation, Technol. Neural Interface*, vol. 16, no. 4, pp. 318–327, 2013.

[11] M. Camilleri *et al.*, "Intra-abdominal vagal blocking (VBLOC therapy): Clinical results with a new implantable medical device," *Surgery*, vol. 143, no. 6, pp. 723–731, 2008.

[12] D. M. Ackermann, Jr., N. Bhadra, M. Gerges, and P. J. Thomas, "Dynamics and sensitivity analysis of high-frequency conduction block," *J. Neural Eng.*, vol. 8, no. 6, p. 065007, 2011.

[13] N. Bhadra and K. L. Kilgore, "High-frequency electrical conduction block of mammalian peripheral motor nerve," *Muscle Nerve*, vol. 32, no. 6, pp. 782–790, Dec. 2005.

[14] C. Tai, D. Guo, J. Wang, J. R. Roppolo, and W. C. de Groat, "Mechanism of conduction block in amphibian myelinated axon induced by biphasic electrical current at ultra-high frequency," *J. Comput. Neurosci.*, vol. 31, no. 3, pp. 615–623, Nov. 2011.

[15] M. C. Bicket, R. Y. Dunn, and S. U. Ahmed, "High-frequency spinal cord stimulation for chronic pain: Pre-clinical overview and systematic review of controlled trials," *Pain Med.*, vol. 17, no. 12, pp. 2326–2336, 2016.

[16] A. Rosenblueth and J. Reboul, "The blocking and deblocking effects of alternating currents on nerve," *Amer. J. Physiol. Legacy Content*, vol. 125, no. 2, pp. 251–264, 1939.

[17] D. M. Ackermann, Jr., E. L. Foldes, N. Bhadra, and K. L. Kilgore, "Effect of bipolar cuff electrode design on block thresholds in high-frequency electrical neural conduction block," *IEEE Trans. Neural Syst. Rehabil. Eng.*, vol. 17, no. 5, pp. 469–477, Oct. 2009.

[18] D. M. Ackermann, Jr., N. Bhadra, E. L. Foldes, X. F. Wang, and K. L. Kilgore, "Effect of nerve cuff electrode geometry on onset response firing in high-frequency nerve conduction block," *IEEE Trans. Neural Syst. Rehabil. Eng.*, vol. 18, no. 6, pp. 658–665, Dec. 2010.

[19] M. Cattell and R. W. Gerard, "The 'inhibitory' effect of high-frequency stimulation and the excitation state of nerve," *J. Physiol.*, vol. 83, no. 4, pp. 407–415, 1935.

[20] J. Reboul and A. Rosenblueth, "The action of alternating currents upon the electrical excitability of nerve," *Amer. J. Physiol. Legacy Content*, vol. 125, no. 2, pp. 205–215, 1939.

[21] J. A. Tanner, "Reversible blocking of nerve conduction by alternating-current excitation," *Nature*, vol. 195, no. 4842, pp. 712–713, 1962.

[22] M. Y. Woo and B. Campbell, "Asynchronous Firing and Block of Peripheral Nerve Conduction by 20 Kc Alternating Current," *Bull. Los Angeles Neurol. Soc.*, vol. 29, pp. 87–94, Jun. 1964.
[23] R. Baratta, M. Ichie, S. K. Hwang, and M. Solomonow, "Orderly stimulation of skeletal muscle motor units with tripolar nerve cuff electrode," *IEEE Trans. Biomed. Eng.*, vol. 36, no. 8, pp. 836–843, Aug. 1989.
[24] B. R. Bowman and D. R. McNeal, "Response of single alpha motoneurons to high-frequency pulse trains," *Stereotactic Funct. Neurosurgery*, vol. 49, no. 3, pp. 121–138, 1987.
[25] C. Tai, J. R. Roppolo, and W. C. de Groat, "Block of external urethral sphincter contraction by high frequency electrical stimulation of pudendal nerve," *J. Urol.*, vol. 172, no. 5, pp. 2069–2072, Nov. 2004.
[26] J. D. Miles, K. L. Kilgore, N. Bhadra, and E. Lahowetz, "Effects of ramped amplitude waveforms on the onset response of high-frequency mammalian nerve block," *J. Neural Eng.*, vol. 4, no. 4, pp. 390–398, 2007.
[27] A. Boger, N. Bhadra, and K. J. Gustafson, "Bladder voiding by combined high frequency electrical pudendal nerve block and sacral root stimulation," *Neurourol. Urodyn.*, vol. 27, no. 5, pp. 435–439, Jun. 2008.
[28] L. Joseph, B. D. Haeffele, and R. J. Butera, "Conduction block induced by high frequency AC stimulation in unmyelinated nerves," in *Proc. 29th Annu. Int. Conf. IEEE Eng. Med. Biol. Soc. (EMBS)*, Aug. 2007, pp. 1719–1722.
[29] D. M. Ackermann, Jr., E. L. Foldes, N. Bhadra, and K. L. Kilgore, "Nerve conduction block using combined thermoelectric cooling and high frequency electrical stimulation," *J. Neurosci. Methods*, vol. 193, no. 1, pp. 72–76, Oct. 2010.
[30] M. Gerges, E. L. Foldes, D. M. Ackermann, Jr., N. Bhadra, N. Bhadra, and K. L. Kilgore, "Frequency- and amplitude-transitioned waveforms mitigate the onset response in high-frequency nerve block," *J. Neural Eng.*, vol. 7, no. 6, p. 066003, 2010.
[31] D. M. Ackermann, Jr., E. L. Foldes, N. Bhadra, and K. L. Kilgore, "Conduction block of peripheral nerve using high-frequency alternating currents delivered through an intrafascicular electrode," *Muscle Nerve*, vol. 41, no. 1, pp. 117–119, Jan. 2010.
[32] D. M. Ackermann, Jr., N. Bhadra, E. L. Foldes, and K. L. Kilgore, "Conduction block of whole nerve without onset firing using combined high frequency and direct current," *Med. Biol. Eng. Comput.*, vol. 49, no. 2, pp. 241–251, Feb. 2011.
[33] D. M. Ackermann, Jr., N. Bhadra, E. L. Foldes, and K. L. Kilgore, "Separated interface nerve electrode prevents direct current induced nerve damage," *J. Neuroscience Methods*, vol. 201, no. 1, pp. 173–176, 2011.
[34] D. M. Ackermann, Jr. *et al.*, "Electrical conduction block in large nerves: High-frequency current delivery in the nonhuman primate," *Muscle Nerve*, vol. 43, no. 6, pp. 897–899, 2011.
[35] H. Liu *et al.*, "Post stimulus effects of high frequency biphasic electrical current on a fibre's conductibility in isolated frog nerves," *J. Neural Eng.*, vol. 10, no. 3, p. 036024, 2013.
[36] G. Yang *et al.*, "Post-stimulation block of frog sciatic nerve by high-frequency (kHz) biphasic stimulation," *Med. Biol. Eng. Comput.*, vol. 55, no. 4, pp. 585–593, 2016.
[37] Y. A. Patel, T. Saxena, R. V. Bellamkonda, and R. J. Butera, "Kilohertz frequency nerve block enhances anti-inflammatory effects of vagus nerve stimulation," *Sci. Rep.*, vol. 7, p. 39810, Jan. 2017.
[38] *Normal Rat Ringer's Solution*. [Online]. Available: http://cshprotocols.cshlp.org/content/2012/2/pdb.rec068312.full?text_only=true
[39] H. Schmalbruch, "Fiber composition of the rat sciatic nerve," *Anatomical Rec.*, vol. 215, no. 1, pp. 71–81, 1986.
[40] S. F. Cogan, "Neural stimulation and recording electrodes," *Annu. Rev. Biomed. Eng.*, vol. 10, pp. 275–309, Aug. 2008.
[41] W. M. Grill and J. T. Mortimer, "Stability of the input-output properties of chronically implanted multiple contact nerve cuff stimulating electrodes," *IEEE Trans. Rehabil. Eng.*, vol. 6, no. 4, pp. 364–373, Dec. 1998.
[42] M. Franke, N. Bhadra, N. Bhadra, and K. Kilgore, "Direct current contamination of kilohertz frequency alternating current waveforms," *J. Neurosci. Methods*, vol. 232, pp. 74–83, Jul. 2014.
[43] K. L. Kilgore and N. Bhadra, "Reversible nerve conduction block using kilohertz frequency alternating current," *Neuromodulation, Technol. Neural Interface*, vol. 17, no. 3, pp. 242–254, Apr. 2014.
[44] P. Aagaard, E. B. Simonsen, J. L. Andersen, P. Magnusson, and P. Dyhre-Poulsen, "Neural adaptation to resistance training: Changes in evoked V-wave and H-reflex responses," *J. Appl. Physiol.*, vol. 92, no. 6, pp. 2309–2318, 2002.
[45] N. Bhadra, E. A. Lahowetz, S. T. Foldes, and K. L. Kilgore, "Simulation of high-frequency sinusoidal electrical block of mammalian myelinated axons," *J. Comput. Neurosci.*, vol. 22, no. 3, pp. 313–326, Jun. 2007.
[46] X. Zhang, J. R. Roppolo, W. C. de Groat, and C. Tai, "Mechanism of nerve conduction block induced by high-frequency biphasic electrical currents," *IEEE Trans. Biomed. Eng.*, vol. 53, no. 12, pp. 2445–2454, Dec. 2006.
[47] C. Tai, W. C. D. Groat, and J. R. Roppolo, "Simulation analysis of conduction block in unmyelinated axons induced by high-frequency biphasic electrical currents," *IEEE Trans. Biomed. Eng.*, vol. 52, no. 7, pp. 1323–1332, Jul. 2005.
[48] H. Liu, J. R. Roppolo, W. C. de Groat, and C. Tai, "The role of slow potassium current in nerve conduction block induced by high-frequency biphasic electrical current," *IEEE Trans. Biomed. Eng.*, vol. 56, no. 1, pp. 137–146, Jan. 2009.
[49] N. A. Pelot, C. E. Behrend, and W. M. Grill, "Modeling the response of small myelinated and unmyelinated axons to kilohertz frequency signals," in *Proc. Int. IEEE/EMBS Conf. Neural Eng. (NER)*, Apr. 2015, pp. 406–409.
[50] B. Howell, L. E. Medina, and W. M. Grill, "Effects of frequency-dependent membrane capacitance on neural excitability," *J. Neural Eng.*, vol. 12, no. 5, pp. 1–17, 2015.
[51] J. Martinek, Y. Stickler, M. Reichel, W. Mayr, and F. Rattay, "A novel approach to simulate Hodgkin–Huxley-like excitation with COMSOL multiphysics," *Artif. Organs*, vol. 32, no. 8, pp. 614–619, Aug. 2008.
[52] S. F. Cogan, P. R. Troyk, J. Ehrlich, and T. D. Plante, "*In vitro* comparison of the charge-injection limits of activated iridium oxide (AIROF) and platinum-iridium microelectrodes," *IEEE Trans. Biomed. Eng.*, vol. 52, no. 9, pp. 1612–1613, Sep. 2005.
[53] E. K. Brunton *et al.*, "*In vivo* comparison of the charge densities required to evoke motor responses using novel annular penetrating microelectrodes," *Frontiers Neurosci.*, vol. 9, p. 265, May 2015.
[54] S. Meijs, M. Fjorback, C. Jensen, S. Sørensen, K. Rechendorff, and N. J. M. Rijkhoff1, "Electrochemical properties of titanium nitride nerve stimulation electrodes: An *in vitro* and *in vivo* study," *Frontiers Neurosci.*, vol. 9, p. 268, Aug. 2015.
[55] L. Kapural *et al.*, "Novel 10-kHz high-frequency therapy (HF10 therapy) is superior to traditional low-frequency spinal cord stimulation for the treatment of chronic back and leg pain: The SENZA-RCT randomized controlled trial," *Anesthesiology*, vol. 123, no. 4, pp. 851–860, 2015.
[56] Y. A. Patel, A. George, A. D. Dorval, J. A. White, D. J. Christini, and R. J. Butera, "Hard real-time closed-loop electrophysiology with the Real-Time eXperiment Interface (RTXI)," *PLoS Comput. Biol.*, vol. 13, no. 5, p. e1005430, 2017. [Online]. Available: https://doi.org/10.1371/journal.pcbi.1005430

Yogi A. Patel (SM'12) was born in Philadelphia, PA, USA, in 1989. He received the B.S. degree in biochemistry/molecular biology and computational science from Mercer University, Macon, GA, USA, in 2011. He is currently pursuing the Ph.D. degree with the Interdisciplinary Bioengineering Graduate Program, Georgia Institute of Technology, Atlanta, GA, USA. His research interests include real-time control systems, neuromodulation, autonomic neurophysiology, and neural control. He is a member of the IEEE Engineering in Medicine and Biology Society, the American Physiology Society, and the Society for Neuroscience. He has received awards for papers and presentations at the IEEE-EMBS, the Neural Interfaces, and the Neuromodulation conferences. He has also received a Young Investigator Award from the IEEE-EMBS.

Brian S. Kim is currently pursing the degree with the Biomedical Engineering Program, Georgia Institute of Technology, Atlanta, GA, USA. His scientific interests are sensory information processing by the central nervous system.

William S. Rountree is currently pursuing the degree with the Mechanical Engineering Program, Georgia Institute of Technology, Atlanta, GA, USA. His scientific interests are design, development, and evaluation of neural interfaces.

Robert J. Butera (SM'03) received the B.E.E. degree from the Georgia Institute of Technology, Atlanta, GA, USA, in 1991, and the Ph.D. degree in electrical and computer engineering from Rice University, Houston, TX, USA, in 1996. Since 1999, he has been with the Faculty, Georgia Tech, where he is currently a Professor and the Co-Director of the Neural Engineering Center. His current research focuses on techniques for peripheral nerve modulation and its application to physiological control. He served the IEEE-EMBS as a member of the AdCom from 2006 to 2010 and as the Vice-President of Finance from 2011 to 2014. He was the Deputy Editor-in- Chief of the IEEE TRANSACTIONS ON BIOMEDICAL CIRCUITS AND SYSTEMS from 2007 to 2010.